JOURNAL OF POLYMER SCIENCE Polymer Chemistry WWW.POLYMERCHEMISTRY.ORG ARTICLE

Synthesis and Electrochromic Properties of Aromatic Polyetherimides Based on a Triphenylamine-dietheramine Monomer

Sheng-Huei Hsiao,[1] Hui-Min Wang,[1] Pei-Chi Chang,[1] Yu-Ruei Kung,[2] Tzong-Ming Lee[2]

[1]Department of Chemical Engineering and Biotechnology, National Taipei University of Technology, Taipei 10608, Taiwan
[2]Division of Organic Opto-Electronic Materials & Applications, Industrial Technology Research Institute, Hsinchu 31040, Taiwan
Correspondence to: S.-H. Hsiao (E-mail: shhsiao@ntut.edu.tw)

Received 10 January 2013; accepted 16 March 2013; published online 17 April 2013
DOI: 10.1002/pola.26686

ABSTRACT: A series of electroactive polyetherimides (PEIs) with triphenylamine (TPA) units were prepared from the polycondensation reactions of 4,4′-bis(*p*-aminophenoxy)triphenylamine with aromatic tetracarboxylic dianhydrides via a conventional two-step technique. The PEIs showed high thermal stability, with glass-transition temperatures of 234–282 °C and decomposition temperatures in excess of 500 °C. They showed well-defined and reversible redox couples during both *p*- and *n*-doping processes, together with multielectrochromic behaviors. These polymers exhibited enhanced redox-stability and electrochromic performance as compared with the corresponding analogs without the phenoxy spacer between the TPA and imide units. © 2013 Wiley Periodicals, Inc. J. Polym. Sci., Part A: Polym. Chem. **2013**, *51*, 2925–2938

KEYWORDS: electrochemistry; electrochromic properties; polyimides; redox polymers; triphenylamine

INTRODUCTION Aromatic polyimides are characterized as highly thermally stable polymers with a favorable balance of physical and chemical properties. They are commercially important materials used extensively as dielectric films and coatings in a wide range of high technology applications.[1] However, rigidity of the backbone and strong interchain interactions result in high melting or glass-transition temperatures (T_g) and limited solubility in most organic solvents. Thus, polyimide processing is generally carried out via poly(amic acid) precursor and then converted to polyimide by vigorous thermal or chemical cyclodehydration. This process has inherent problems such as emission of volatile by-products and storage instability of poly(amic acid) solution. To overcome these problems, many attempts have been made to the synthesis of soluble and processable polyimides in fully imidized form while maintaining their excellent properties.[2] The majority of methods used for improving the solubility while maintaining the high-temperature performance of polyimides have involved the structural modifications of dianhydride and diamine monomers. Typical approaches include the introduction of flexible linkages, kinked or unsymmetrical structures, bulky packing-disruptive units, and bulky lateral groups into the polymer backbone.[3]

Triarylamines are an important class of aromatic compounds because they can form stable aminium radical cations. They can be building blocks for high-spin polyradicals that showed ferromagnetic coupling.[4] Perhaps most commonly, triarylamines have been used as the hole-transport layer in electroluminescent devices,[5,6] because the two-layered organic electroluminescent device using a diamine as a hole-transfer layer was first reported by Tang and VanSlyke[7] in 1987. Particularly, solution processability and good film formation properties of triarylamine-based polymers may render them suitable for the fabrication of large-area and flexible electronics based on spin-coating and inkjet printing.[8] In addition, triarylamine-based polymers also show interesting electrochromic behavior upon electrochemical oxidation.[9] In recent years, Liou and coworkers have carried out extensive studies on the design and synthesis of triarylamine-based high-performance polymers such as aromatic polyimides[10] and polyamides[11] for potential electrochromic applications. The triarylamine-containing monomers such as diamines and dicarboxylic acids could be easily prepared using a well-established procedure, and they could react with the corresponding comonomers through conventional polycondensation techniques, producing the desired triarylamine-based polymers. In general, these polymers exhibit good solubility to organic solvents due to the introduction of bulky, packing-disruptive triarylamine moieties. Thus, they could be readily solution-cast into flexible electrochromic films with good mechanical property and high thermal stability. Thus, incorporation of three-dimensional, packing-disruptive triarylamine units into the polyimide backbone not only resulted in

Additional Supporting Information may be found in the online version of this article.

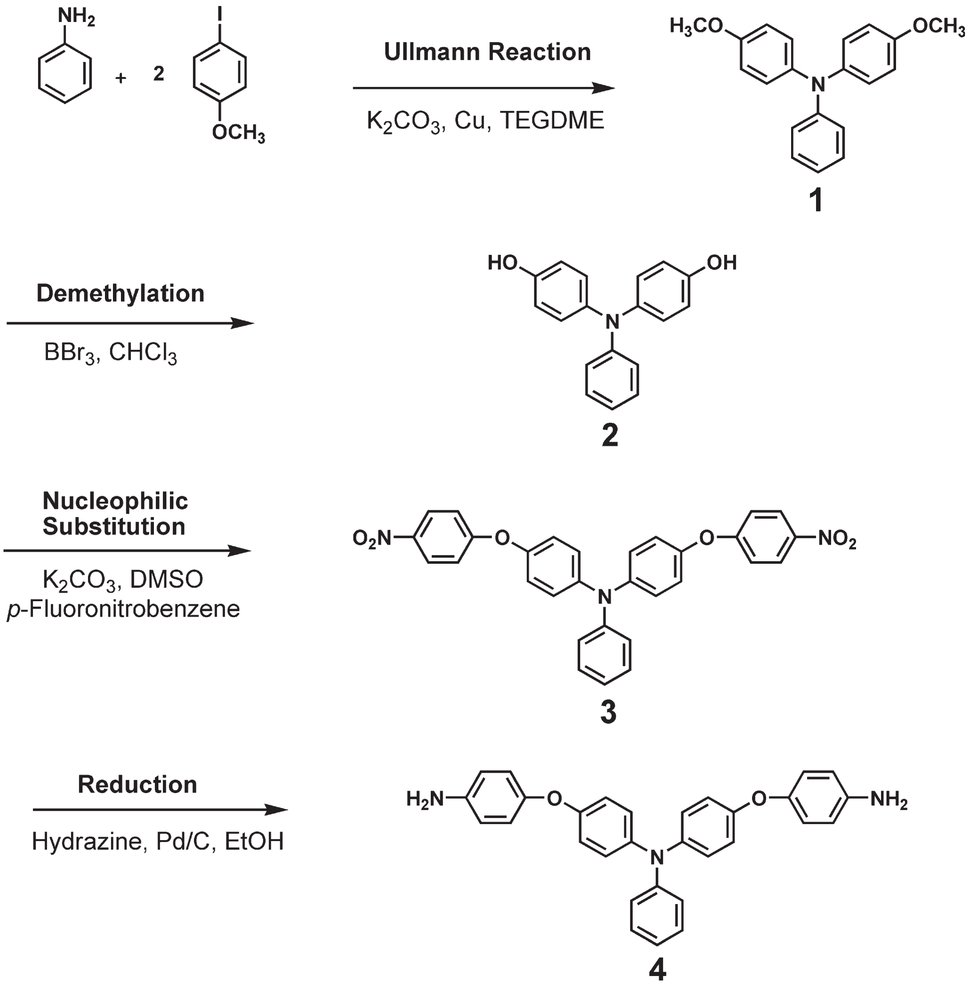

SCHEME 1 Synthetic route to the target TPA-dietheramine monomer **4**.

enhanced solubility but also led to new electronic functions of polyimides such as electrochromic characteristics.[12]

It has been demonstrated that triarylamine-based polyimides generally exhibited poor electrochemical and electrochromic stability as compared with their polyamide analogs because of the strong electron-withdrawing imide group, which increases the oxidation potential of the triarylamine unit and destabilizes the resultant amino radical cation upon oxidation.[10(b),11(c)] Incorporating a spacer between the triarylamine core and the imide ring may improve the electrochemical and elcetrochromic stability of this kind of electroactive polymers. Thus, a triphenylamine (TPA)-based dietheramine monomer, namely 4,4′-bis(*p*-aminophenoxy)triphenylamine, was synthesized and led to a series of polyetherimides (PEIs) with main-chain TPA and phenoxy groups. By the incorporation of the phenoxy spacer between the TPA and imide units, the resulting PEIs are expected to exhibit enhanced electrochemical and electrochromic properties. Although this dietheramine has been synthesized previously and one of its derived polyimides has been studied for potential applications in volatile polymeric memory devices,[13] the electrochemical and electrochromic properties of this kind polyimides have not been well understood.

EXPERIMENTAL

Materials

Aniline (Acros), 4-iodoanisole (Acros), potassium carbonate (K_2CO_3, Showa), triethylene glycol dimethyl ether (TEGDME, Acros), copper (Cu, Acros), boron tribromide (BBr_3, Acros), sodium hydrogen carbonate ($NaHCO_3$, Showa), *p*-fluoronitrobenzene (Acros), 10% palladium on charcoal (Pd/C, Fluka), and hydrazine monohydrate (TCI) were used as received. Dimethyl sulfoxide (DMSO, Tedia), *N,N*-dimethylformamide (DMF, Acros), *N,N*-dimethylacetamide (DMAc, Fluka), pyridine (Py, Wako), and *N*-methyl-2-pyrrolidone (NMP, Tedia) were dried over calcium hydride for 24 h, distilled under reduced pressure, and stored over 4 Å molecular sieves in a sealed bottle. The dietheramine monomer 4,4′-bis(*p*-aminophenoxy)triphenylamine (**4**) was synthesized starting from the Ullmann reaction between aniline and 4-iodoanisole by a four-step reaction sequence. The synthetic details and characterization have been included in the Supporting Information. Commercially available tetracarboxylic dianhydrides such as pyromellitic dianhydride (PMDA; **5a**; Aldrich) and 3,3′,4,4′-benzophenonetetracarboxylic dianhydride (BTDA; **5c**; Aldrich) were purified by recrystallization from acetic anhydride. 3,3′,4,4′-Biphenyltetracarboxylic dianhydride

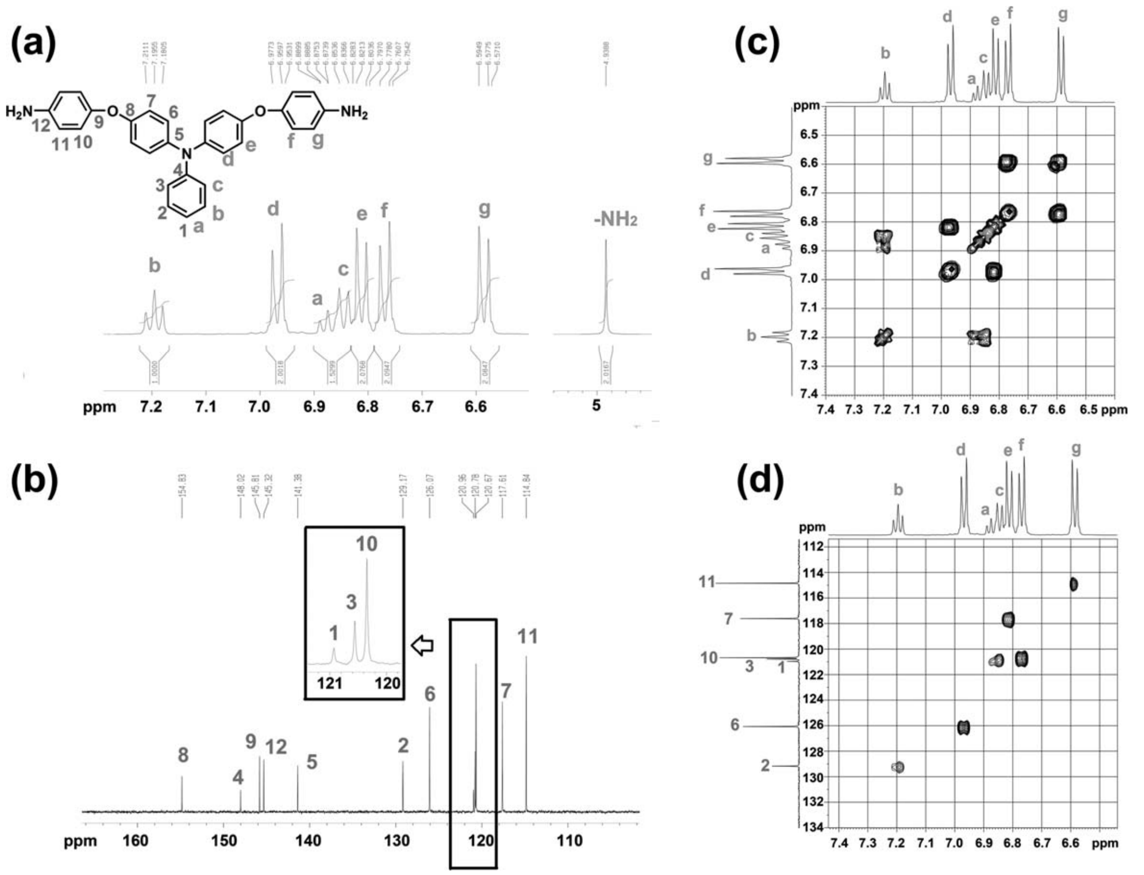

FIGURE 1 (a) ^{1}H NMR, (b) ^{13}C NMR, (c) H—H COSY, and (d) C—H HMQC spectra of the target dietheramine monomer **4** in DMSO-d_6.

(BPDA; **5b**; Oxychem), 4,4′-oxydiphthalic dianhydride (ODPA; **5d**; Oxychem), 3,3′,4,4′-diphenylsulfonetetracarboxylic dianhydride (DSDA; **5e**; New Japan Chemical), and 2,2-bis(3,4-dicarboxyphenyl)hexafluoropropane dianhydride (6FDA; **5f**; Hoechst Celanese) were heated at 250 °C *in vacuo* for 3 h before use. Tetrabutylammonium perchlorate, Bu_4NClO_4, were recrystallized from ethyl acetate under nitrogen atmosphere and then dried *in vacuo* prior to use. All other reagents and solvents were used as received from commercial sources.

Polymer Synthesis

PEIs **6a–6f** were synthesized from TPA-dietheramine **4** and aromatic dianhydrides **5a–5f** by the conventional two-step method via thermal or chemical imidization reaction. A typical procedure is as follows. The dietheramine monomer **4** (0.5085 g, 1.106 mmol) was dissolved in 9.5 mL of DMAc in a 50-mL round-bottom flask. Then **5f**, 6FDA (0.4915 g, 1.106 mmol) was added to the diamine solution in one portion. Thus, the solid content of the solution is ~10 wt %. The mixture was stirred at room temperature for about 18 h to yield a viscous poly(amic acid) solution. The inherent viscosity of the resulting poly(amic acid) was 1.39 dL/g, measured in DMAc at a concentration of 0.50 g/dL at 30 °C. The poly(amic acid) film was obtained by casting from the reaction polymer solution onto a glass Petri dish and drying at 90 °C overnight. The poly(amic acid) in the form of solid film was converted to PEI **6f** by successive heating under vacuum at 150 °C for 1 h, 200 °C for 1 h, and then 300 °C for 1 h.

For the chemical imidization method, 4 mL of acetic anhydride and 2 mL of Py were added to a poly(amic acid) solution obtained by a similar process as above, and the mixture was heated at 100 °C for 1 h to effect a complete imidization. The homogenous polymer solution was poured slowly into 150 mL of stirring methanol giving rise to light yellow precipitate that was collected by filtration, washed thoroughly with hot water and methanol, and dried. A polymer solution was made by the dissolution of about 0.5 g of the polyimide sample in 10 mL of hot DMAc. The homogeneous solution was poured into a 7-cm glass Petri dish, which was placed in a 90 °C oven overnight for the slow release of the solvent, and then the film was stripped off from the glass substrate and further dried in vacuum at 160 °C for 6 h.

Measurements

Infrared (IR) spectra were recorded on a Horiba FT-720 FTIR spectrometer. ^{1}H and ^{13}C NMR spectra were measured on a Bruker AVANCE 500 FT-NMR system with tetramethylsilane as an internal standard. The inherent viscosities were determined with a Cannon-Fenske viscometer at 30 °C. Wide-angle X-ray diffraction (WAXD) measurements were

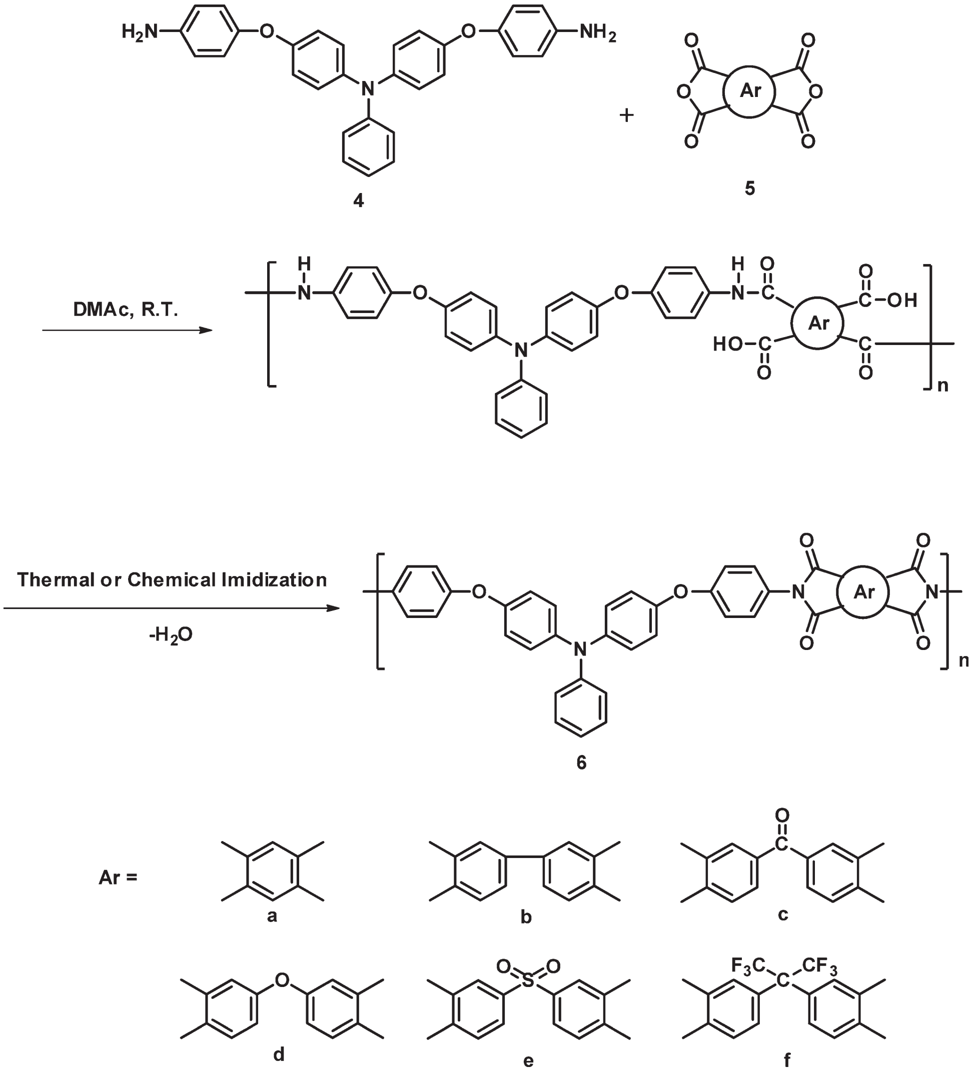

SCHEME 2 Synthesis of PEIs **6a–6f**.

performed at room temperature (ca. 25 °C) on a Shimadzu XRD-6000 X-ray diffractometer with a graphite monochromator (operating at 40 kV and 30 mA), using nickel-filtered Cu-Kα radiation ($\lambda = 1.5418$ Å). The scanning rate was 2°/min over a range of $2\theta = 10$–$40°$. Thermogravimetric analysis (TGA) was performed with a Perkin-Elmer Pyris 1 TGA. Experiments were carried out on ~4–6 mg of samples heated in flowing nitrogen or air (flow rate = 40 cm^3/min) at a heating rate of 20 °C/min. DSC analyses were performed on a Perkin-Elmer Pyris 1 DSC at a scan rate of 20 °C/min in flowing nitrogen. Thermomechanical analysis (TMA) was determined with a Perkin-Elmer TMA 7 instrument. The TMA experiments were carried out from 50 to 400 °C at a scan rate of 10 °C/min with a penetration probe 1.0 mm in diameter under an applied constant load of 10 mN. Softening temperatures (T_s) were taken as the onset temperatures of probe displacement on the TMA traces. Electrochemistry was performed with a CHI 750A electrochemical analyzer. Cyclic voltammetry (CV) was conducted with the use of a three-electrode cell in which ITO (polymer films area about 0.8 × 1.25 cm^2) was used as a working electrode. A platinum wire was used as an auxiliary electrode. All cell potentials were taken with the use of a home-made Ag/AgCl, KCl (sat.) reference electrode. Ferrocene was used as an external reference for calibration (+0.48 V vs. Ag/AgCl). Voltammograms are presented with the positive potential pointing to the left and with increasing anodic currents pointing downwards. Spectroelectrochemistry analyses were carried out with an electrolytic cell, which was composed of a 1 cm cuvette, ITO as a working electrode, a platinum wire as an auxiliary electrode, and Ag/AgCl reference electrode. Absorption spectra in the spectroelectrochemical experiments were measured with an Agilent 8453 UV–vis diode array spectrophotometer.

RESULTS AND DISCUSSION

Monomer Synthesis

The target aromatic dietheramine monomer, 4,4′-bis(*p*-aminophenoxy)triphenylamine (**4**), was synthesized starting from aniline and 4-iodoanisole by a four-step reaction

TABLE 1 Inherent Viscosity and Solubility[a] Behavior of PEIs Prepared via Thermal (−T) or Chemical (−C) Imidization

	η_{inh} (dL/g)[b]		Solvents[c]					
Polymer Code	PAA[d]	Polyimide	NMP	DMAc	DMF	DMSO	*m*-Cresol	THF
6a-T	1.59	−		−	−	−	−	−
6a-C		−	+−	+−	+−	+−	+−	+−
6b-T	1.82	−	−	−	−	−	+−	−
6b-C		−	+−	+−	+−	+−	+−	+−
6c-T	1.36	−	+−	+−	−	−	+−	−
6c-C		1.10[e]	++	+−	+−	+−	+−	+−
6d-T	1.61	−	−	−	−	−	+−	−
6d-C		0.82[e]	++	+−	+−	+−	+	+−
6e-T	1.53	−	+−	+−	+−	+−	+−	−
6e-C		0.90	++	++	+	+	+	+−
6f-T	1.39	−	−	−	+−	+−	+−	+−
6f-C		0.65	++	++	+	+	+	+

[a] The qualitative solubility was tested with 10 mg of a sample in 1 mL of stirred solvent. ++: soluble at room temperature; +: soluble on heating; +−: partially soluble; −: insoluble even on heating.

[b] Inherent viscosity measured at a concentration of 0.5 dL/g in DMAc at 30 °C.

[c] Solvent:NMP: *N*-methyl-2-pyrrolidone; DMAc: *N*,*N*-dimethylacetamide; DMF: *N*,*N*-dimethylformamide; DMSO: dimethyl sulfoxide; THF: tetrahydrofuran.

[d] PAA = Poly(amic acid).

[e] Inherent viscosity measured at a concentration of 0.5 dL/g in NMP at 30 °C.

sequence as depicted in Scheme 1. The intermediate compound 4,4′-dimethoxytriphenylamine (**1**) was synthesized via Ullmann reaction between aniline and 4-iodoanisole by using copper powder and K_2CO_3 in TEGDME. According to a literature method,[14] demethylation of the dimethoxy compound **1** with boron tribromide gave 4,4′-dihydroxytriphenylamine (**2**). Then, 4,4′-bis(*p*-nitrophenoxy)triphenylamine (**3**) was prepared by the nucleophilic aromatic fluoro-displacement reaction of *p*-fluoronitrobenzene with compound **2** in the presence of K_2CO_3. The target dietheramine monomer **4** was prepared by hydrazine Pd/C-catalyzed reduction of dinitro compound **3.** FTIR, ^{1}H NMR, and ^{13}C NMR spectroscopic techniques were used to identify structures of the intermediate compounds **1**, **2**, and **3** and the target dietheramine monomer **4.** Figure S1 (see Supporting Information) illustrates FTIR spectra of all the synthesized compounds. The methyl groups of compound **1** give rise to a symmetric stretching vibration at about 2834 cm^{-1} and an asymmetric stretch at about 2929 cm^{-1}. After demethylation to compound **2**, the characteristic absorption of the phenol group (—OH stretching) appears in the region of 3100–3500 cm^{-1}. The nitro groups (—NO_2 asymmetric and symmetric stretching) of compound **3** give two strong bands at around 1589 and 1344 cm^{-1}. After reduction, the characteristic absorptions of the nitro group disappear and the amino group shows the typical N—H stretching absorption pair at 3463 and 3365 cm^{-1} as shown in the IR spectrum of compound **4**. The NMR spectra of all the intermediate compounds are included in Supporting Information Figures S2–S4. ^{1}H NMR, ^{13}C NMR, and two-dimensional (2-D) NMR spectra of the target TPA-dietheramine **4** are compiled in Figure 1. The ^{1}H and ^{13}C NMR spectra of **4** are essentially identical to those reported in a previous publication,[13] where the intermediate dinitro compound **3** has been prepared by a different synthetic route. Only a slight difference in chemical shifts of the resonance peaks was observed due to the use of different test solvents. The ^{1}H NMR spectra confirm that the nitro groups have been completely transformed into amino groups by the high field shift of the aromatic protons and the resonance signals at around 5.0 ppm corresponding to the amino protons. Assignments of each carbon and proton assisted by the 2-D NMR spectra are also indicated in these spectra, and they are in good agreement with the proposed molecular structure of **4**.

Polymer Synthesis

PEIs **6a–6f** were prepared in conventional two-step method by the reactions of dietheramine **4** with various aromatic dianhydrides (**5a–5f**) to form poly(amic acid)s, followed by thermal or chemical cyclodehydration (Scheme 2). As shown in Table 1, the poly(amic acid) precursors had inherent viscosities in the range of 1.36–1.82 dL/g. The molecular weights of these poly(amic acid)s were sufficiently high to permit the casting of flexible and tough poly(amic acid) films, which were subsequently converted into tough PEI films by stage-by-stage heating to elevated temperatures. The transformation from poly(amic acid) to a polyimide could also be carried out via chemical cyclodehydration by using acetic anhydride and Py. All the PEIs showed the characteristic absorption bands of the imide ring near 1780 (asymmetric C=O stretching) and 1732 cm^{-1} (symmetric C=O stretching). Typical IR spectra of PEI **6c** and its poly (amic acid) precursor are illustrated in Supporting Information Figure S5. The ^{1}H NMR spectrum of a representative PEI **6f** is illustrated in Figure 2. All the aromatic protons in

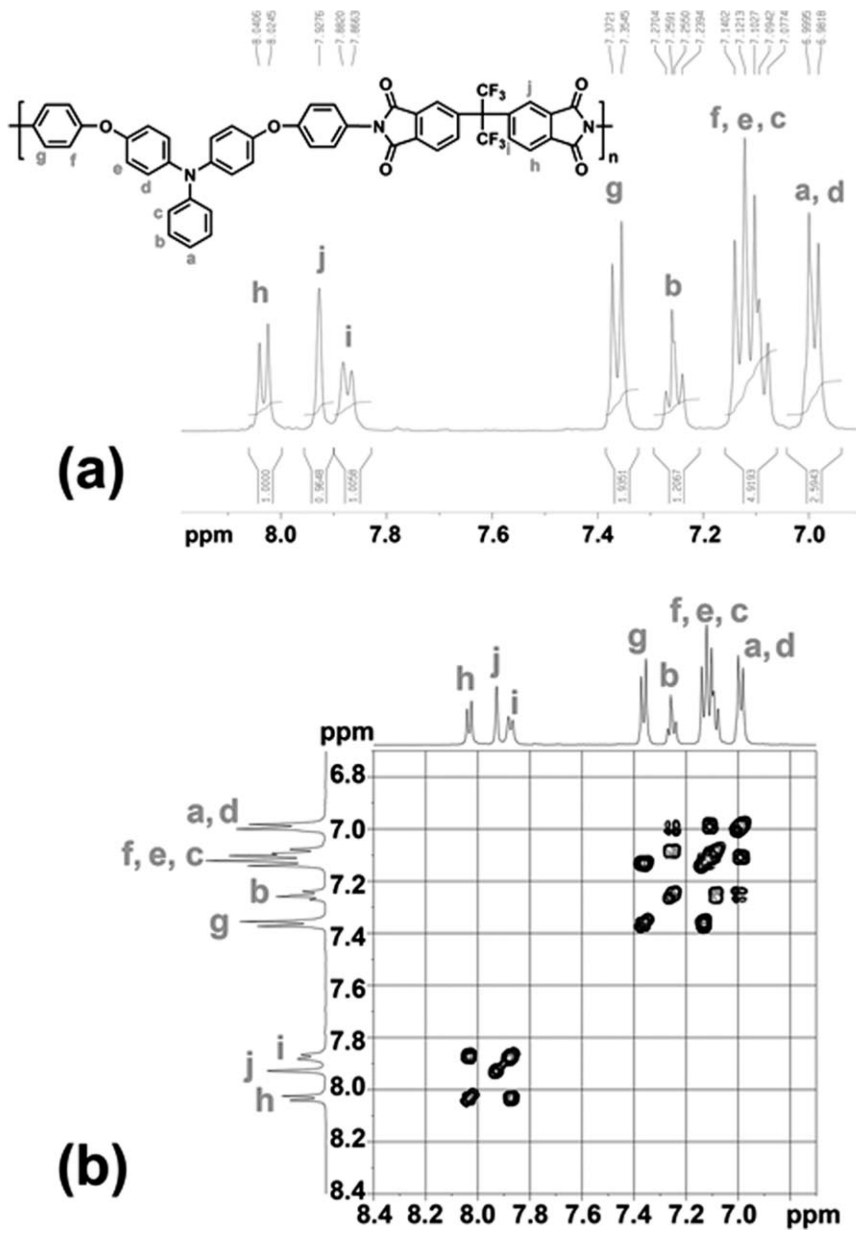

FIGURE 2 (a) ^{1}H NMR and (b) H—H COSY spectra of PEI **6f** in $CDCl_3$.

the dietheramine moiety resonated in the region of δ 6.98–8.02 ppm, and the protons in the 6FDA component appeared at a lower field of 7.88–8.02 ppm. Assignments of each proton, assisted by the 2-D NMR spectroscopy, are in good agreement with the structure of the repeating unit.

Polymer Properties

Basic Characterization

As evidenced by their WAXD patterns (see Supporting Information Figure S6), the PEIs exhibited an amorphous nature. Their amorphous properties can be attributed to the incorporation of packing-disruptive TPA unit along the polymer backbone, which results in a high steric hindrance for close packing, and thus reduces their crystallization tendency.

The solubility behaviors of all the PEIs prepared by both of thermal and chemical imidization methods are summarized in Table 1. All the thermally imidized samples did not reveal good solubility to the tested solvents. However, the PEIs prepared by the chemical imidization method exhibited an increased solubility as compared with those by the thermal imidization method. The chemically imidized samples of the PEIs derived from less stiff dianhydrides such as **6c** to **6f** are soluble at least in NMP at room temperature. PEIs **6e** and **6f** are also soluble in DMAc. The lower solubility of the

TABLE 2 Thermal Properties of PEIs

Polymer[a] Code	T_g (°C)[b]	T_s (°C)[c]	T_d at 5% Weight Loss (°C)[d]		T_d at 10% Weight Loss (°C)[d]		Char Yield (wt %)[e]
			N_2	Air	N_2	Air	
6a	282	282	563	544	590	587	62
6b	246	242	589	576	609	612	64
6c	247	241	562	570	585	606	63
6d	234	231	597	598	610	622	59
6e	264	260	510	524	543	567	54
6f	258	257	569	552	590	579	65

[a] All the polymer films were heated at 300 °C for 1 h to DSC and TGA experiments.

[b] Midpoint temperature of the baseline shift on the second DSC heating trace (rate = 20 °C/min) of the sample after quenching from 400 to 50 °C (rate = 200 °C/min) in nitrogen.

[c] Softening temperature measured by TMA with a constant applied load of 10 mN at a heating rate of 10 °C/min.

[d] Decompositiontemperature at which a 5 or 10% weight loss was recorded by TGA at a heating rate of 20 °C/min and a gas flow rate of 20 cm^3/min.

[e] Residual wt % at 800 °C at a scan rate 20 °C/min in nitrogen.

thermally cured samples may be attributed to the presence of partial interchain crosslinking or an aggregation of the polymer chains during thermal curing process.

Thermal Properties

The thermal stability and phase-transition temperatures of these PEIs were determined by TGA, DSC, and TMA techniques. The thermal behavior data of PEIs **6a–6f** are included in Table 2. Typical TGA and TMA curves of the representative **6f** are shown in Figure 3. All of the PEIs exhibited a similar TGA pattern with no significant weight loss below 500 °C in air or nitrogen atmosphere. The decomposition temperatures (T_d) at which a 10% weight-loss temperatures of the aromatic PEIs in nitrogen and air were recorded in the range of 543–610 °C and 567–622 °C, respectively. The amount of carbonized residue (char yield) of these polymers in nitrogen atmosphere was more than 54% at 800 °C. The high char yields of these polymers can be ascribed to their high aromatic content. The glass-transition temperatures (T_g) of all the polymers were observed in the range of 234–282 °C by DSC (Supporting Information Figure S7) and decreased with decreasing rigidity and symmetry of the aromatic tetracarboxylic dianhydride. The decreasing order of T_g generally correlated with that of chain flexibility. For example, PEI **6d** from ODPA showed the lowest T_g of 234 °C because of the presence of flexible ether linkage between the phthalimide units. The softening temperatures (T_s; may be referred to as apparent T_g) of the polymer film samples were determined by the TMA method with a loaded penetration probe. They were obtained from the onset temperature of the probe displacement on the TMA trace. A typical TMA thermogram for PEI **6f** is illustrated in the inset of Figure 3. In most cases, the T_s values of the PEIs obtained by TMA are comparable to the T_g values measured by the DSC experiments.

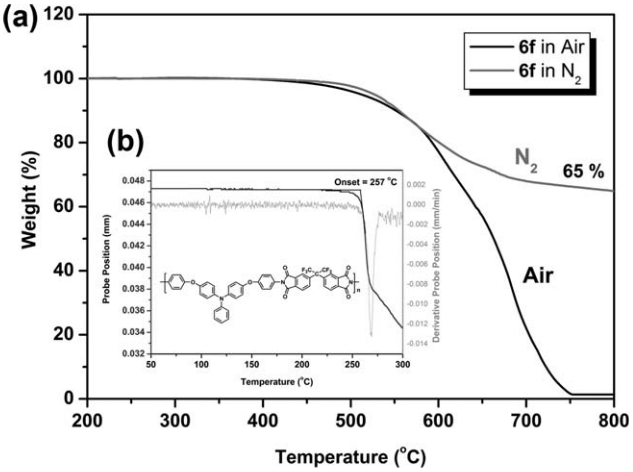

FIGURE 3 TMA and TGA curves of PEI **6f** with a heating rate of 10 and 20 °C/min, respectively.

Electrochemical Properties

The electrochemical properties of the PEIs were investigated by CV conducted for the cast films on an ITO-coated glass substrate as working electrode in dry acetonitrile (CH_3CN; for the anodic scan) or DMF (for the cathodic scan) containing 0.1 M of Bu_4NClO_4 as an electrolyte under nitrogen atmosphere. The first CV scans of the **6a–6f** series PEIs are depicted in Figure 4, and the data are summarized in Table 3. As shown in Table 3, the oxidation half-wave potentials ($E_{1/2}^{ox}$) were recorded in the range of 0.96–0.99 V. One pair of reversible redox waves are observed for all the PEIs in the oxidation region, which are attributed to the oxidation of TPA units. These PEIs also show two or three quasireversible waves in the reduction region because of the reduction of imide segments. Redox reactions for the diimide systems shown in Supporting Information Figure S8 represent a possible distribution of electron density for the reduced forms and describe by other resonance forms, which contribute to the charge delocalization. Reduction of the imide groups may

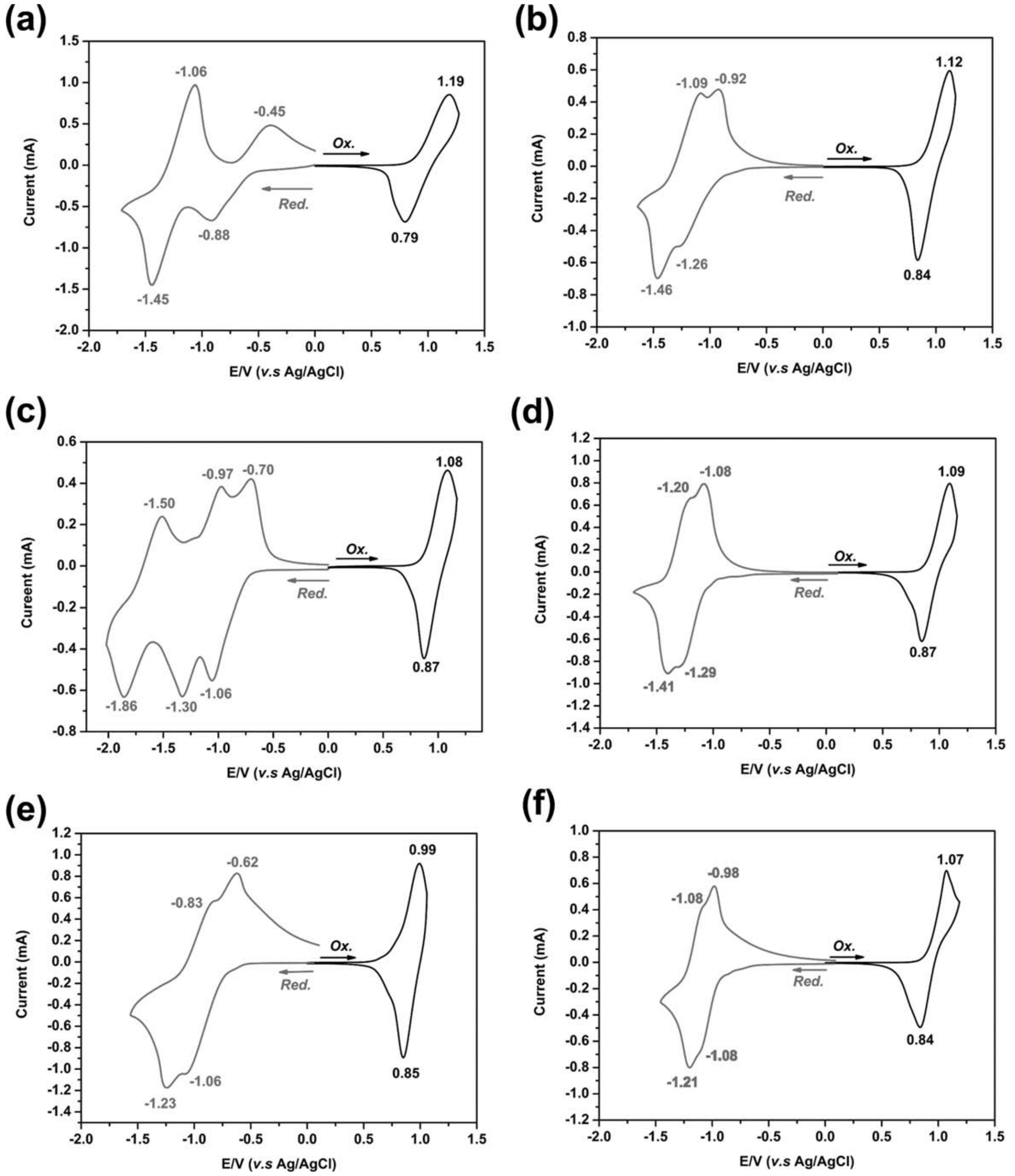

FIGURE 4 Cyclic voltammetric diagrams of the cast films of PEIs (a) **6a**, (b) **6b**, (c) **6c**, (d) **6d**, (e) **6e**, and (f) **6f** on an ITO-coated glass substrate in 0.1 M Bu_4NClO_4 acetonitrile (for anodic process) and DMF (for cathodic process) solution at a scan rate of 50 and 100 mV/s, respectively.

induce increased quinoid character due to charge separation by the ring structure to minimize the electron–electron repulsion. The CV curve of PMDA PEI **6a** [Fig. 4(a)] shows that the pyromellitimide groups undergo two quasireversible one-electron reductions, which occurred at $E_{pc} = -0.88$ and -1.45 V. The first reduction corresponds to formation of radical anions, and the second reduction relates to formation of dianions (see Supporting Information Figure S8). Similar result was observed with the BPDA PEI **6b** [Fig. 4(b)]; however, the first reduction process ($E_{pc} = -1.26$ V) occurred at a more negative potential than observed for the PMDA PEI **6a**. Two separated reduction peaks peculiar to the BPDA diimide segment indicate a facile electronic communication between the two phthalimide groups. It is worth to note that the benzophenone diimide group of the BTDA PEI **6c** revealed three reversible redox couples [Fig. 4(c)]. It was proposed that the first two electroreduction processes occur for the BTDA diimide units, leading to the radical-anion ($E_{pc} = -1.06$ V) and diradical-dianion form ($E_{pc} = -1.30$ V), respectively. The benzophenone moiety allows a third

TABLE 3 Optical and Electrochemical Properties of PEIs

	Thin Film (nm)		Oxidation Potential (V)[a]		Reduction Potential (V)[b]				Bandgap (eV)[c]		Energy level (eV)[e]	
Polymer Code	λ_{max}^{Abs}	λ_{onset}^{Abs}	E_{onset}^{OX}	$E_{1/2}^{OX}$	E_{onset}^{red}	$E_{1/2}^{red1}$	$E_{1/2}^{red2}$	$E_{1/2}^{red3}$	E_g^{opt}	E_g^{ec}	HOMO	LUMO
6a	296	606	0.88	0.99	−0.57	−0.67	−1.26	–	2.04	1.66	5.35	3.69
6b	299	557	0.89	0.98	−0.81	−1.09	−1.28	–	2.22	2.07	5.34	3.27
6c	299	583	0.85	0.98	−0.73	−0.88	−1.14	−1.68	2.12	1.86	5.34	3.48
6d	296	531	0.88	0.98	−1.06	−1.25	–	–	2.33	2.23	5.34	3.11
6e	298	547	0.78	0.97	−0.75	−0.84	−1.03	–	2.26	1.81	5.33	3.52
6f	296	506	0.90	0.96	−0.95	−1.10	–	–	2.45	2.06	5.32	3.26
6′d	305	590	1.00	1.08	−1.02	−0.79	–	–	2.10	1.64	5.51	3.87

[a] Verus Ag/AgCl in CH3CN. $E_{1/2}$ = average potential of the redox couple peaks.

[b] Versus Ag/AgCl in DMF.

[c] Bandgaps calculated from absorption edge of the polymer films: $E_g^{opt} = 1{,}240/\lambda_{onset}$.

[d] E_g^{ec}, electrochemical band gap is derived from the difference between HOMO and LUMO values.

[e] The HOMO and LUMO energy levels were calculated from $E_{1/2}^{ox}$ and $E_{1/2}^{red}$ values of CV curves and were referenced to ferrocene (4.8 eV relative to the vacuum energy level).

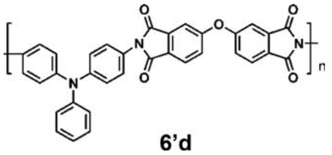

6’d

electroreduction to the proposed radical–trianion form ($E_{pc} = -1.86$ V) as depicted in Supporting Information Figure S8. Two pair of redox waves were observed for the imide reduction of ODPA polyimide **6d** [Fig. 4(d)], DSDA polyimide **6e** [Fig. 4(e)], and 6FDA polyimide **6f** [Fig. 4(f)] during the negative CV scanning, even though the conjugation across the imide group is disrupted by the ether, sulfonyl, and hexafluoroisopropylidene linker.

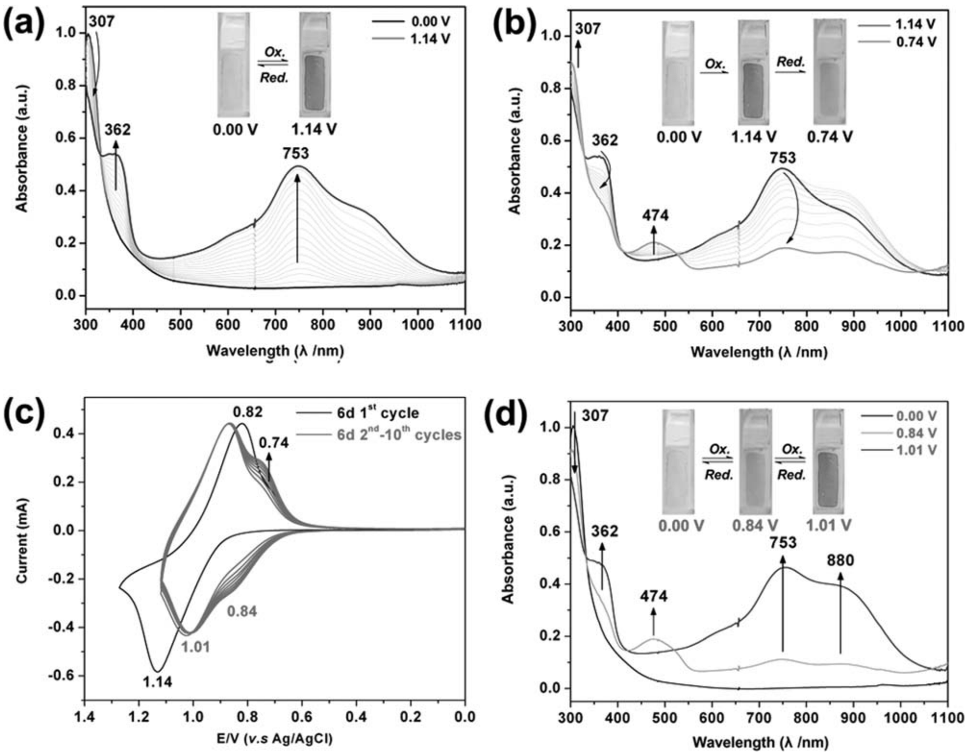

FIGURE 5 (a) Absorption spectra of the thin film of PEI **6d** on an ITO electrode at various potentials from 0 to 1.14 V, (b) spectral change from 1.14 back to 0.74 V, (c) repetitive cyclic voltammograms for **6d**, and (d) the second spectroelectrochemical series of the **6d** thin film.

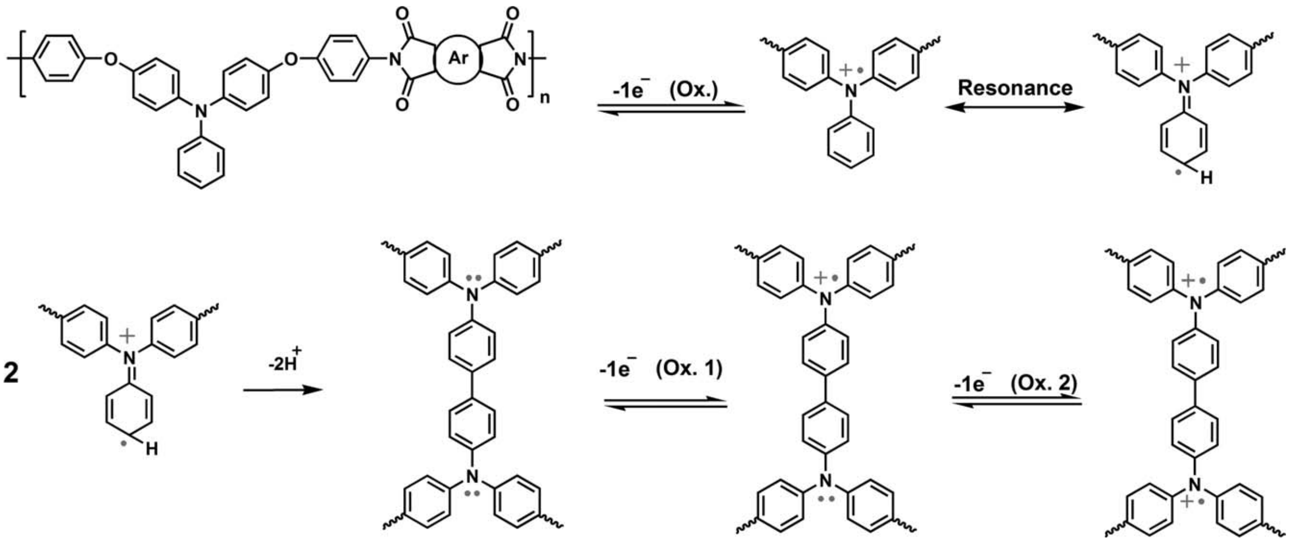

SCHEME 3 Proposed coupling reaction between the TPA units and the subsequent oxidation reactions in the PEIs.

When comparing the CV diagram of PEI **6d** with that of analogous **6′d** (Supporting Information Fig. S9), it is found that incorporation of a phenoxy group between the TPA and imide groups results in a decreased oxidation potential. This is likely attributed to the decreased electron-withdrawing effect of the imide group caused by the insertion of the phenoxy spacer and possibly also to the electron-donating nature of the phenoxy group. Furthermore, it was found that all the PEIs revealed new redox patterns upon repetitive scanning over the voltage range from 0 to 1.1 V. An example of PEI **6d** is shown in Figure 5(c). For the first positive potential scan, we observed an oxidation peak at about 1.14 V. From the first reverse negative scan, we detected one cathodic peak at 0.82 V together with a shoulder at 0.74 V. After the second scan, a new oxidation shoulder appeared at 0.84 V that was complementary anodic process of the shoulder at 0.74 V in the first reverse negative scan. In the meantime, the oxidation peak revealed a decreased current and moved to a lower anodic potential (1.01 V). The observation of a new oxidation couple in the second potential scan implies that the TPA radical cations were involved in fast electrochemical/chemical reactions that produced a structure that was easier to oxidize than was the parent TPA unit. In addition, it was also found that the value of the anodic current intensity at 0.84 V slightly increased with the number of the scan. This is a typical oxidation wave of the tetraphenylbenzidine (TPB) group, indicating the occurrence of the oxidative coupling between TPA units (Scheme 3). The electro-oxidation of TPA was extensively studied in the pioneering works reported by Adams, Nelson, and coworkers.[15] All those studies concluded that the radical cation formed by oxidation is involved in a dimerization reaction that produced TPB. The TPB has a lower oxidation potential than TPA because of its more extended π-electron delocalization.

Spectroelectrochemistry and Electrochromic Switching

When the PEI films were electrochemically oxidized or reduced, a strong color change of them was observed. Their electrochromic properties were further studied by the means of electrochromic absorbance spectra with a potential step scan on the polymer films coated on an ITO electrode via a combination of a potentiostat and an UV–vis-NIR spectrometer. In this case, a three-electrode configuration was still used for applying potential to the polymer films. During the test, the electrochromic absorbance spectra were recorded. As a typical example, the result of the **6d** film upon electro-oxidation (*p*-doping) is presented in Figure 5(a) as a series of UV–vis-NIR absorption curves correlated to electrode potentials. In the neutral form, PEI **6d** exhibited strong absorption at wavelength around 307 nm, characteristic for TPA, but it almost transmissive in the visible region. When the applied voltage was stepped from 0 to 1.14 V, the intensity of the absorption peak around 307 nm decreased gradually, and new peaks at 362 and 753 nm gradually increased in intensity. Consequently, the film turned from colorless to blue. We attribute these spectral changes to the formation of a stable cation radical of the TPA moiety. As shown in Figure 5(b), when the applied voltage returned from 1.14 to 0.74 V, the absorbance peak at 362 and 753 nm was decreased dramatically while a new absorption band at 474 nm appeared. Meanwhile, the film changed color from blue to pale orange. For the explanation of this spectral change, repetitive CV diagrams of **6d** are also included in Figure 5(c). After the first electrochemical series of PEI **6d** was recorded from 0 to 1.14 V and then back to 0 V, we reapplied the electrode voltage and recorded its absorption profile. As shown in Figure 5(d), an additional pale orange oxidized state has been observed in the re-scan film at applied voltage of 0.84 V. The film showed a multicolored electrochromism from colorless neutral state to pale orange and blue oxidized states. This phenomenon persisted for several subsequent scans. The

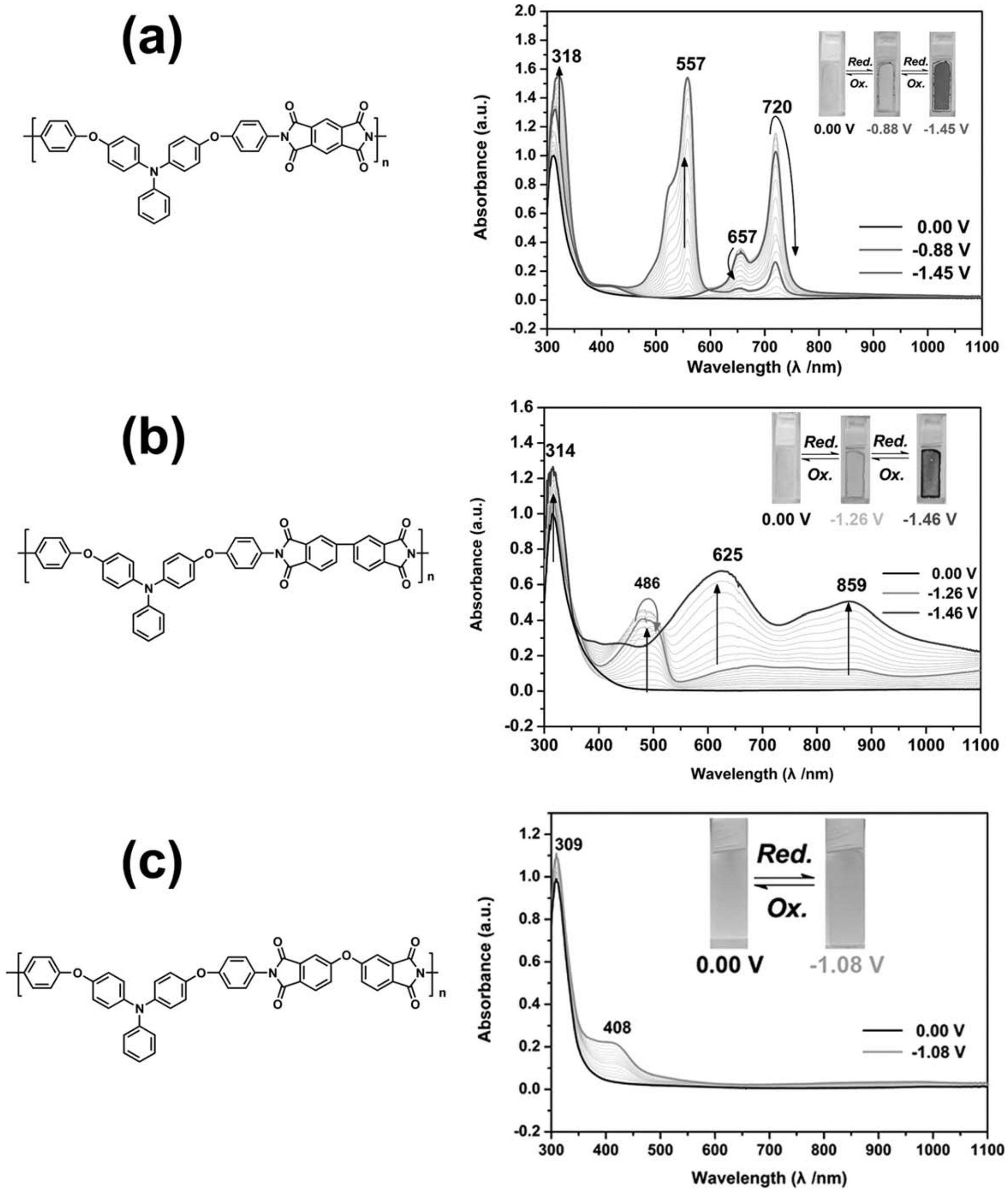

FIGURE 6 Spectroelectrochemistry of the films of PEIs (a) **6a**, (b) **6b,** and (c) **6d** on an ITO electrode in 0.1 M Bu_4NClO_4/DMF at various applied potentials.

new pale orange oxidized state may be attributed to the oxidation of the benzidine unit resulted from the coupling reaction of TPA units, as shown in Scheme 3. As shown in Supporting Information Figure S9, a pale orange coloring state was also observed in the second spectroelectrochemical series of the referenced polyimide **6′d**. This result indicated the occurrence of the oxidative coupling between the TPA units of **6′d** in the electrochemical oxidation process, although the oxidation waves could not be well-resolved in the CV analysis.

Figure 6 shows the spectral changes of the cast films of PEIs **6a, 6b,** and **6d** upon electroreduction (*n*-doping). The radical anion of PEI **6a**, which appears at potential −0.88 V, exhibits a strong band at 318 nm and an increased absorption between 657 and 720 nm. As shown in the inset of Figure 6(a), the radical anion form of polyimide **6a** is light green in color. Further reduction at potentials negative to −1.45 V results in the two-electron reduced (dianion) state with a new strong absorption at 557 nm, and the film turns to a pink color during the second-step reduction. The spectral

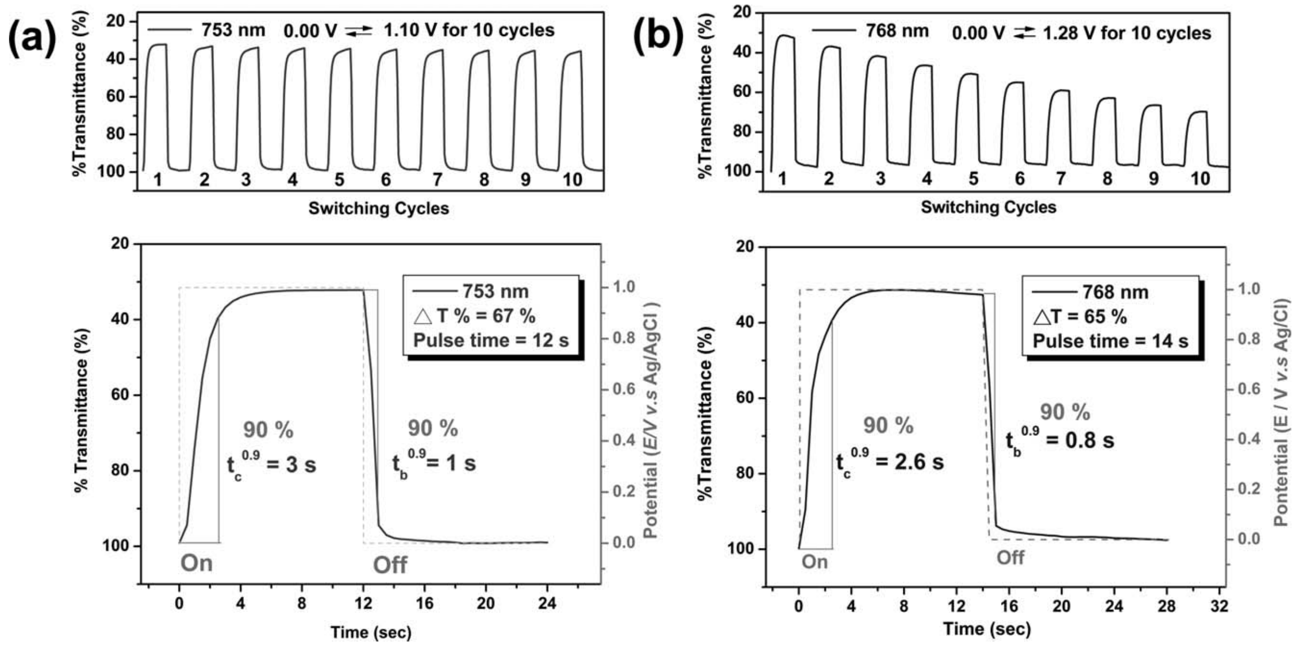

FIGURE 7 Potential step absorptiometry of the cast films of PEI **6d** and the referenced **6′d** on the ITO-glass slide (coated area – 1 cm^2; in CH_3CN with 0.1 M Bu_4NClO_4 as the supporting electrolyte) by applying a potential step: (a) optical switching for **6d** at potential 0.0 V$\rightleftharpoons$1.10 V and cycle time 12 s, monitored at $\lambda_{max} = 753$ nm; (b) **6′d** at potential 0.0 V$\rightleftharpoons$1.28 V and cycle time 14 s, monitored at $\lambda_{max} = 768$ nm.

changes associated with the electroreduction reactions of the pyromellitimide unit are very similar to that of standard PMDA-ODA polyimide (ODA: 4,4′-oxydianiline) reported by Mazur et al.[16] This result reaffirms that the diamine residue has very little direct influence on the reduction of the diimide moiety as reported in literature.[16] The radical anion of PEI **6b** formed at −1.26 V reveals a new absorption band in the visible region at about 486 nm, and the film appears as yellow-green in color [Fig. 6(b)]. As the film was further charged with electrons at−1.46 V, the absorption intensity at 486 nm decreased, and two new bands emerged at about 625 and 859 nm, and the film turned to a blue color during the second-step reduction. Figure 6(c) illustrates the spectral and coloration changes of PEI **6d** on electroreduction. However, the color change (colorless to light yellow) is not strong as that observed for PEIs **6a** and **6b**. All the polyimide films showed a quick optical contrast loss after about 10 full switches. It is believed that a little unwanted delamination or dissolution of the anionic products in the DMF/electrolyte solution is the main cause of the unstable switching behavior. The electrochemical and optical properties of the PEI films on electrochemical reduction are summarized in the Supporting Information Table S1.

To obtain a partially crosslinked film of PEI **6d**, the film of **6d** on ITO-glass was repeatedly scanned between 0.00 and 1.10 V at 100 mV/s for 10 cycles. After that, the spectroelectrochemistry and electrochromic switching of the electrochromic film was investigated. The spectroelectrochemical behavior of the polyimide film was found to be very similar to that shown in Figure 5(d). Electrochromic switching studies for the PEIs were performed to monitor the percent transmittance changes ($\Delta T\%$) as a function of time at their absorption maximum (λ_{max}) and to determine the response time by stepping potential repeatedly between the neutral and oxidized states. The active area of the polymer film on ITO glass is about 1 cm^2. Figure 7 depicts the optical transmittance at 753 nm as a function of time by applying square-wave potential steps between 0.00 and 1.10 V for a resident time of 12 s for PEI **6d** and at 768 nm between 0.00 and 1.28 V for a resident time of 14 s for the referenced polyimide **6′d**. The PEI film of **6d** almost showed no optical contrast loss during the first 10 switching cycles; however, the **6′d** film showed a moderate optical contrast loss after 10 full switches. The response time was calculated at 90% of the full-transmittance change, because it is difficult to perceive any further color change with naked eye beyond this point. As shown in Figure 7(a), PEI **6d** attained 90% of a complete coloring and bleaching in 3 and 1 s, respectively. The optical contrast measured as $\Delta T\%$ of PEI **6d** between neutral colorless and oxidized blue states was found to be 67% at 753 nm. Figure 7(b) indicates that the referenced polyimide **6′d** attained 90% of a complete coloring and bleaching in 2.6 and 0.8 s, respectively. The optical contrast measured as $\Delta T\%$ of polyimide **6′d** between neutral colorless and oxidized blue states was found to be 65% at 768 nm. The electrochromic coloring efficiency (CE) for the blue coloring ($\eta = \triangle OD_{753}/Q$) of the PEI **6d** was estimated to be 178 cm^2/C, but that for the blue coloring ($\eta = \triangle OD_{768}/Q$) of the polyimide **6′d** was estimated to be only 51 cm^2/C (Table 4).

As mentioned earlier, the PEI **6a** also exhibited a strong coloration change upon electrochemical reduction. Supporting Information Figure S10 shows the optical transmittance

TABLE 4 Electrochromic Properties of PEIs **6a**, **6d**, and **6′d**

			Response Time[b]				
Polymer	λ_{max}[a] (nm)	$\Delta\%T$	t_c (s)	t_b(s)	ΔOD[c]	Q_d[d] (mC/cm^2)	CE[e] (cm^2/C)
6d-*p*-doping	753	67	3	1	0.376	2.11	178
6′d-*p*-doping	768	65	2.6	0.8	0.363	7.10	51
6a-*n*-doping	558	95	5.2	2.3	2.093	11.23	186

[a] Wavelength of absorption maximum.

[b] Time for 90% of the full-transmittance change.

[c] Optical Density (ΔOD) = log[$T_{bleached}/T_{colored}$], where $T_{colored}$ and $T_{bleached}$ are the maximum transmittance in the oxidized and neutral states, respectively.

[d] Q_d is ejected charge, determined from the *in situ* experiments.

[e] Coloration efficiency (CE) = ΔOD/Q_d.

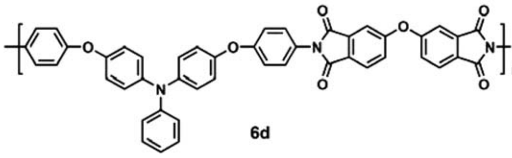

6d

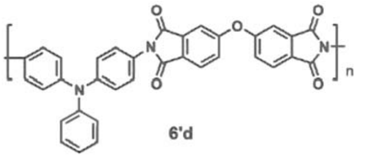

6′d

changes at $\lambda_{max} = 558$ nm of PEI **6a** while switching between its colorless (neutral) and pink (reduced) states in 0.1 M Bu_4NClO_4/DMF by applying a potential step between 0.00 and −1.45 V (vs. Ag/AgCl). The electrochromic properties of the **6a** film during n-doping processes are also summarized in Table 4. In general, the cathodically coloring switching is less stable than the anodically coloring switching for this PEI film. A faster decay in optical contrast and an earlier delamination of the polymer film were usually observed for these PEIs during the cathodically switching experiments.

CONCLUSIONS

Herein, we synthesized and characterized a series of electroactive PEIs from 4,4′-bis(*p*-aminophenoxy)triphenylamine and various aromatic dianhydrides. Insertion of a phenoxy spacer between the TPA unit and the imide ring decreases the oxidation potentials and increases the electrochemical stability of the polyimides. All the PEIs exhibit an ambipolar electrochemical and electrochromic behavior. When the polymer film was subjected to a repeated cyclic scan between 0 and 1.1 V, an electrochemical coupling reaction between the TPA units occurred which may lead to a partially crosslinked film. The PEI films exhibit reversible electrochemical oxidation accompanied by strong color changes that can be switched through modulation of the applied potential. Thus, these characteristics suggest that these PEIs may find applications in electrochromic devices.

REFERENCES AND NOTES

1 (a) Polyimides; D. Wilson, H. D. Stenzenberger, P. M. Hergenrother, Eds.; Blackie: Glasgow and London, **1990**; (b) C. E. Sroog, *Prog. Polym. Sci.* **1991**, *16*, 561–694; (c) Polyimides: Fundamentals and Applications; M. K. Ghosh, K. L. Mittal, Eds.; Marcel Dekker: New York, **1996**; (d) D.-J. Liaw, K.-L. Wang, Y.-C. Huang, K.-R. Lee, J.-Y. Lai, C.-S. Ha, *Prog. Polym. Sci.* **2012**, *37*, 907–974.

2 For review papers: see (a) S. J. Huang, A. E. Hoyt, *TRIP* **1995**, *3*, 262–271; (b) J. de Abajo, J. G. de la Campa, *Adv. Polym. Sci.* **1999**, *140*, 23–59; (c) M. Ding, *Prog. Polym. Sci.* **2007**, *32*, 623–668; (d) M. G. Dhara, S. Banerjee, *Prog. Polym. Sci.* **2010**, *35*, 1022–1077.

3 For selected examples: see (a) S.-H. Hsiao, K.-H. Lin, *J. Polym. Sci. Part A: Polym. Chem.* **2005**, *43*, 331–341; (b) S. M. Kwak, J. H. Yeon, T. H. Yoon, *J. Polym. Sci. Part A: Polym. Chem.* **2006**, *44*, 2567–2578; (c) Y.-T. Chern, J.-Y. Tsai, J.-J. Wang, *J. Polym. Sci. Part A: Polym. Chem.* **2009**, *47*, 2443–2452; (d) C. W. Chung, C. H. Lin, P. W. Cheng, H. J. Hwang, S. Dai, *J. Polym. Sci. Part A: Polym. Chem.* **2009**, *47*, 2486–2499; (e) S. J. Zhang, Y. F. Li, T. Ma, J. J. Zhao, X. Y. Xu, F. C. Yang, X. Y. Xiang, *Polym. Chem.* **2010**, *1*, 485–493; (f) Y. Liu, Y. Xing, Y. H. Zhang, S. W. Guan, H. B. Zhang, Y. Wang, Y. P. Wang, Z. H. Jiang, *J. Polym. Sci. Part A: Polym. Chem.* **2010**, *48*, 3281–3289; (g) M. Calle, A. E. Lozano, J. G. de la Campa, J. de Abajo, *Macromolecules* **2010**, *43*, 2268–2275; (h) C. H. Lin, S. L. Chang, P. W. Cheng, *J. Polym. Sci. Part A: Polym. Chem.* **2011**, *49*, 1331–1340; (i) H. B. Wei, X. L. Pei, X. Z. Fang, *J. Polym. Sci. Part A: Polym. Chem.* **2011**, *49*, 2484–2494; (j) S.-H. Hsiao, H.-M. Wang, W.-J. Chen, T.-M. Lee, C.-M. Leu, *J. Polym. Sci. Part A: Polym. Chem.* **2011**, *49*, 3109–3120; (k) Y. J. Hou, G. F. Chen, X. L. Pei, X. Z. Fang, *J. Polym. Res.* **2012**, *19*, 9955.

4 (a) A. Ito, H. Ino, K. Tanaka, K. Kanemoto, T. Kato, *J. Org. Chem.* **2002**, *67*, 491–498; (b) E. Fukuzaki, H. Nishide, *Org. Lett.* **2006**, *8*, 1835–1838.

5 (a) Y. Shirota, *J. Mater. Chem.* **2000**, *10*, 1–25; (b) Y. Shirota, *J. Mater. Chem.* **2005**, *15*, 75–93; (c) Y. Shirota, H. Kageyama, *Chem. Rev.* **2007**, *107*, 953–1010.

6 M. Thelakkat, *Macromol. Mater. Eng.* **2002**, *287*, 442–461.

7 C. W. Tang, S. A. VanSlyke, *Appl. Phys. Lett.* **1987**, *51*, 913–915.

8 (a) R. Tang, Z. Tan, Y. Li, F. Xi, *Chem. Mater.* **2006**, *18*, 1053–1061; (b) Y.-H. Kim, Q. Zhao, S.-K. Kwon, *J. Polym. Sci. Part A: Polym. Chem.* **2006**, *44*, 172–182; (c) Q. Kong, D. Zhu, Y. Quan, Q. Chen, J. Ding, J. Lu, Y. Tao, *Chem. Mater.* **2007**, *19*, 3309–3318; (d) J. A. Mikroyannidis, K. M. Gibbons, A. P. Kulkarni, S.

A. Jenekhe, *Macromolecules* **2008**, *41*, 663–674; (e) J. H. Park, C. Yun, M. H. Park, Y. Do, S. Yoo, M. H. Lee, *Macromolecules*, **2009**, *42*, 6840–6843; (f) C.-Y. Lin, Y.-C. Lin, W.-Y. Hung, K.-T. Wong, R.-C. Kwong, S. C. Xia, Y.-H. Chen, C.-I. Wu, *J. Mater. Chem.* **2009**, *19*, 3618–3626.

9 (a) M.-Y. Chou, M.-k. Leung, Y. O. Su, C. L. Chiang, C.-C. Lin, J.-H. Liu, C.-K. Kuo, C.-Y. Mou, *Chem. Mater.* **2004**, *16*, 654–661; (b) S. Beaupre, J. Dumas, M. Leclerc, *Chem. Mater.* **2006**, *18*, 4011–4018; (c) J. Natera, L. Otero, L. Sereno, F. Fungo, N.-S. Wang, Y.-M. Tsai, T.-Y. Hwu, K.-T. Wong, *Macromolecules* **2007**, *40*, 4456–4463; (d) J. Natera, L. Otero, F. D'Eramo, L. Sereno, F. Fungo, N.-S. Wang, Y.-M. Tsai, K.-T. Wong, *Macromolecules* **2009**, *42*, 626–635.

10 (a) S.-H. Cheng, S.-H. Hsiao, T.-H. Su, G.-S. Liou, *Macromolecules* **2005**, *38*, 307–316; (b) S.-H. Hsiao, Y.-M. Chang, H.-W. Chen, G.-S. Liou, *J. Polym. Sci. Part A: Polym. Chem.* **2006**, *44*, 4579–4592; (c) G.-S. Liou, S.-H. Hsiao, H.-W. Chen, *J. Mater. Chem.* **2006**, *16*, 1831–1842; (d) H.-M. Wang, S.-H. Hsiao, *Polymer* **2009**, *50*, 1692–1699; (e) S.-H. Hsiao, G.-S. Liou, Y.-C. Kung, H.-Y. Pan, C.-H. Kuo, *Eur. Polym. J.* **2009**, *45*, 2234–2248; (f) Y.-C. Kung, S.-H. Hsiao, *J. Mater. Chem.* **2011**, *21*, 1746–1754; (g) Y.-C. Kung, W.-F. Lee, S.-H. Hsiao, G.-S. Liou, *J. Polym. Sci. Part A: Polym. Chem.* **2011**, *49*, 2210–2221.

11 (a) C.-W. Chang, G.-S. Liou, S.-H. Hsiao, *J. Mater. Chem.* **2007**, *17*, 1007–1015; (b) S.-H. Hsiao, G.-S. Liou, Y.-C. Kung, H.-J. Yen, *Macromolecules* **2008**, *41*, 2800–2808; (c) Y.-C. Kung, G.-S. Liou, S.-H. Hsiao, *J. Polym. Sci. Part A: Polym. Chem.* **2009**, *47*, 1740–1755; (d) S.-H. Hsiao, G.-S. Liou, H.-M. Wang, *J. Polym. Sci. Part A: Polym. Chem.* **2009**, *47*, 2330–2343; (e) S.-H. Hsiao, G.-S. Liou, Y.-C. Kung, Y.-M. Chang, *J. Polym. Sci. Part A: Polym. Chem.* **2010**, *48*, 2798–2809; (f) S.-H. Hsiao, G.-S. Liou, Y.-C. Kung, T.-J. Hsiung, *J. Polym. Sci. Part A: Polym. Chem.* **2010**, *48*, 3392–3401; (g) H.-M. Wang, S.-H. Hsiao, G.-S. Liou, C.-H. Sun, *J. Polym. Sci. Part A: Polym. Chem.* **2010**, 48, 4775–4789; (h) H.-M. Wang, S.-H. Hsiao, *J. Polym. Sci. Part A: Polym. Chem.* **2011**, *49*, 337–351; (i) Y.-C. Kung, S.-H. Hsiao, *J. Polym. Sci. Part A: Polym. Chem.* **2011**, *49*, 3475–3490.

12 H.-J. Yen, G.-S. Liou, *Polym. Chem.* **2012**, *3*, 255–264.

13 T. Kuorosawa, C.-C. Chueh, C.-L. Liu, T. Higashihara, M. Ueda, W.-C. Chen, *Macromolecules* **2010**, *43*, 1236–1244.

14 (a) M. Thelakkat, C. Schmitz, C. Hohle, P. Strohriegl, H.-W. Schmidt, U. Hofmann, S. Schloter, D. Haarer, *Phys. Chem. Chem. Phys.* **1999**, *1*, 1693–1698; (b) M. Faccini, M. Balakrishnan, M. B. Diemeer, Z. p. Hu, K. Clays, I. Asselberghs, A. Leinse, A. Driessen, D. N. Reinhoudt, W. Verboom, *J. Mater. Chem.* **2008**, *18*, 2141–2149.

15 (a) E. T. Seo, R. F. Nelson, J. M. Fritsch, L. S. Marcoux, D. W. Leedy, R. N. Adams, *J. Am. Chem. Soc.* **1966**, *88*, 3498–3503; (b) R. F. Nelson, R. N. Adams, *J. Am. Chem. Soc.* **1968**, *90*, 3925–3930; (c) S. C. Creason, J. Wheeler, R. F. Nelson, *J. Org. Chem.* **1972**, *37*, 4440–4446.

16 S. Mazur, P. S. Lugg, C. Yarnitzky, *J. Electrochem. Soc.* **1987**, *134*, 346–353.